



1 **Combining colour parameters and geochemical tracers to improve sediment source discrimination**
2 **in a mining catchment (New Caledonia, South Pacific Islands)**

3 Virginie Sellier¹, Oldrich Navratil², John Patrick Lacey³, Cédric Legout⁴, Michel Allenbach⁵, Irène

4 Lefèvre¹, Olivier Evrard¹

5 ¹Laboratoire des Sciences du Climat et de l'Environnement (LSCE), UMR 8212 (CEA/CNRS/UVSQ-IPSL),

6 Université Paris-Saclay, Gif-sur-Yvette (France)

7 ²Laboratoire Environnement Ville Société (EVS), Université Lumière Lyon 2, UMR 5600 (CNRS), Lyon

8 (France)

9 ³Alberta Environment and Parks, Calgary, Alberta (Canada)

10 ⁴Institut des Géosciences de l'Environnement (IGE), UMR 5001, Grenoble (France)

11 ⁵LIVE-EA 4243, Université de Nouvelle-Calédonie & LABEX Corail, Nouméa (Nouvelle-Calédonie,

12 France)

13 **Corresponding author:** selliervirg@free.fr ; Tel: (33)673910072



14 **Abstract**

15 Over the last century, human activities have induced significant land-cover changes that have
16 accelerated soil erosion processes around the world. In New Caledonia, a French island located in the
17 south-west Pacific Ocean, open-cast nickel mining has raised many concerns regarding its impact on
18 riverine systems (i.e. hyper-sedimentation, overburden) and the island's ecosystems (i.e. flooding,
19 lagoon siltation, water pollution).

20 A sediment tracing study has been conducted to quantify the contribution of mining versus
21 non-mining sub-catchments in one of the first areas exploited for nickel mining, the Thio River
22 catchment (397 km²). Sediment deposited during two cyclonic events (i.e. 2015 and 2017) was
23 collected following a tributary design approach. Source (n= 24) and river sediment (n= 19) samples
24 were analyzed by X-ray fluorescence and spectroscopy in the visible spectra (i.e. 365-735 nm). Four
25 fingerprinting approaches based on (1) colour parameters, (2) geochemical properties, (3) colour
26 parameters coupled with geochemical properties and (4) the entire visible spectrum were tested to
27 estimate sediment source contributions.

28 The results demonstrated that the individual sediment tracing methods based on spectroscopy
29 measurements (i.e. (1) and (4)) did not provide sufficient discrimination between sources. However,
30 the inclusion of colour properties in addition to geochemical parameters (3) provided the highest
31 discrimination between sources (i.e. 92.6 % of source variance explained). Although with a slightly
32 lower discrimination potential (i.e. 83.1 % of variance explained in sources), the geochemical
33 approach (2) provided similar results to those obtained with the colour coupled with geochemical
34 approach (3). In addition, mixed linear models associated with these two approaches have been
35 experimentally validated with artificial mixture samples. The results obtained with model (3) showed
36 that mining source contributions strongly dominated the sediments inputs with a mean contribution
37 of 68 % (SD 25 %) for the 2015 flood event and 88 % (SD 8%) for the 2017 flood event. These results
38 suggest that catchment management should focus on the contributions of mining tributaries to



39 reduce sediment inputs in the river systems. Therefore, the use of these approaches based on
40 geochemical properties individually (2) and coupled to colour parameters (3) could be extended to
41 other mining catchments of New Caledonia but also to other similar nickel mining catchments
42 around the world (e.g. Australia, Brazil, Dominican Republic, Cuba) to estimate sediment source
43 apportionment.

44

45 **Keywords:** Nickel mining • Sediment source fingerprinting • Soil erosion • Modeling

46



47 Introduction

48 At the dawn of a fourth industrial revolution, demand for metalliferous minerals continues to
49 increase and impact the world market (Prior et al., 2013;Highley et al., 2004). Currently, open-cast
50 mining generates more than three-quarters of the world's metal ores. However, the extraction of
51 these minerals is associated with deleterious impacts on the environment. In particular, these mines
52 are responsible for the increase in soil erosion and the transfer of sediment in river systems
53 worldwide (Yellishetty et al., 2013;Dumas et al., 2010;Abel et al., 2000).

54 New Caledonia, an island located in the south-western Pacific Ocean and currently the world's
55 sixth-largest producer of nickel, is in particular challenged with the problems of hyper-sedimentation
56 and over-burden of its river systems. Several studies outline how mining activities, which started in
57 1875, are generally responsible for these deleterious river morphological changes (Bird et al.,
58 1984;Iltis, 1992;Garcin et al., 2017). The excessive sediment inputs transferred mainly during
59 extreme rainfall events (e.g. cyclones and tropical depressions) lead to the increased occurrence of
60 flooding events in these tropical regions. Owing to the occurrence of major cyclones in New
61 Caledonia (i.e. on average one cyclone every 2.7 years (Garcin, 2010)), the local population regularly
62 have to deal with the damage generated by these flood events (e.g. damage to human settlements,
63 public infrastructure, agricultural land and, human casualties). Moreover, the island's agricultural and
64 fishing resources are also impacted.

65 Suspended sediment is known to transport large quantities of contaminants in river systems
66 (Vaithyanathan et al., 1993;Bradley and Lewin, 1982). Hedouin et al. (2007), and more recently
67 Baudrimont et al. (2019), observed high concentrations of trace metals, including Ni and Cr, in
68 marine and freshwater organisms in New Caledonia. On a more global level, this anthropogenic
69 activity also threatens the second largest coral reef in the world, listed as a UNESCO World Heritage.
70 In particular, the increased turbidity associated with sediment supply could disrupt coral metabolism
71 (i.e. photosynthetic processes) (Juillot, 2019). These coral reefs provide an exceptional biological



72 diversity and deliver several essential ecosystem services to the local population including fisheries,
73 coastal protection and tourism (Pascal, 2010). The implementation of effective and perennial
74 sediment control measures on mining sites (e.g. sediment retention basin, revegetation) is therefore
75 required to reduce sediment inputs into the lagoon.

76 Erosion generated by open-cast nickel mining (i.e. mining bare soil, mining roads, mining
77 prospection and mining waste) do not provide the only sediment source in New Caledonia's mining
78 catchments. The use of fires to clear landscapes conducted by the local population for farming,
79 pasture and hunting increase the area of bare soils (Dumas et al., 2010). Soils that are left uncovered
80 by vegetation are more sensitive to erosion and they may be exposed to shallow landsliding (Blake et
81 al., 2009; Smith et al., 2011). Moreover, several invasive species such as deers or wild pigs also
82 threaten soil stability through trampling and overgrazing (Shellberg et al., 2010).

83 The contribution of mining tributaries (i.e. draining mining areas) and non-mining tributaries
84 (i.e. draining areas without mining activities) to sediment transiting catchments in New Caledonia
85 therefore needs to be discriminated. This discrimination has particularly become important since the
86 mining industries are subject to the "polluter pays" principle applied since 1975, i.e. the obligation to
87 fund remediation according to the extent of the damage generated by mining activity on the
88 environment. There is therefore a real social, environmental and financial challenge in discriminating
89 between sediment sources generated by mining activities and other potential sediment sources.

90 Sediment fingerprinting techniques have been developed since the 1970s to determine the
91 spatial origin of sediment sources and quantify their contributions (Collins et al., 1996; Walling et al.,
92 1979). These techniques are based on the analysis of multiple conservative properties both in the
93 sediments and their potential sources. Fallout radionuclides (Wallbrink, 2004; Evrard et al.,
94 2015; Wallbrink et al., 1998; Evrard et al., 2020), geochemical (Collins et al., 1997; Laceby and Olley,
95 2015) and mineral properties (Klages and Hsieh, 1975; Walden et al., 1997) are the most frequently
96 used tracers to quantify sediment source contributions. The use of fallout radionuclides and



97 geochemical properties as potential tracers was investigated to quantify the sources of suspended
98 sediment in the Thio River catchment (397 km²), one of the first catchments in New Caledonia to be
99 mined for nickel. Geochemical properties provided promising results (i.e. 83.1 % of variance
100 explained in sources) while the fallout radionuclides proved to be unsuitable (i.e. non-discriminatory)
101 (Sellier et al., 2019). However, other less expensive, faster and possibly more efficient techniques
102 than the more conventional methods previously tested could be envisaged. For example,
103 spectroscopy in the mid-infrared (MIR) (Poulenard et al., 2009), the visible near-infrared (VNIR) and
104 the shortwave-infrared (SWIR) (Brosinsky et al., 2014) regions of spectra have been used to quantify
105 the sediment source contributions. It is also non-destructive and requires low quantities of sample
106 material. Spectroscopy could therefore meet both the need for a simple and rapid sediment tracing
107 method in a context where flood events are frequent.

108 Moreover, New Caledonia has a specific geological feature which is at the origin of its mineral
109 wealth: one third of its surface area is covered with peridotite massifs. The weathering of these rocks
110 enriched in Fe and transition metals such as Mn, Ni, Cr and Co results in the formation of Ni- and Fe-
111 rich smectite, serpentine, goethite and hematite. The oxidized minerals (i.e. goethite and hematite)
112 provide a particularly reddish-orange colour to mining sources that distinguishes them from non-
113 mining sources, which tend to be grey in colour. The differences made visually between the two
114 sources further encourage the analysis of sources by spectroscopy and especially spectroscopy in the
115 visible region of the spectrum (i.e. 365-735 nm). In particular, the colorimetric parameters derived
116 from the visible spectrum have been shown to be effective in discriminating sediment sources. Their
117 discrimination power has been tested both individually (Evrard et al., 2019; Martínez-Carreras et al.,
118 2010; Uber et al., 2019) and in combination with other tracers (e.g. geochemical properties (Tiecher
119 et al., 2015)) according to the conventional fingerprinting approach (i.e. statistical analysis and use of
120 a mixing model). A more alternative approach based on the entire visible spectrum with the partial
121 least square regression (PLSR) models has also been developed to trace origin of sediment sources in
122 the literature (Legout et al., 2013; Tiecher et al., 2015).



123 As part of this study, four sediment fingerprinting methods based on (1) colour parameters, (2)
124 geochemical properties, (3) colour parameters coupled with geochemical properties and (4) PLSR
125 models based on the whole visible spectrum were tested in the Thio River catchment. Source (n=24)
126 and river sediment (n=19) samples were collected following a tributary design approach and
127 analyzed by X-ray fluorescence and spectroscopy in the visible spectra (i.e. 365-735 nm). The
128 performance of each method to estimate sediment source contributions was evaluated in order to
129 select the best technique to be applied in the Thio River catchment and possibly in other mining
130 catchments of New Caledonia. On a wider scale, the tracers retained in this study could be
131 considered as potential sedimentary tracers to estimate sediment source apportionment in other
132 similar nickel mining catchments around the world (e.g. Australia, Brazil, Dominican Republic, Cuba).

133 Materials and methods

134 **1.1.Study area**

135 Located in the southwestern Pacific Ocean, New Caledonia (18 500 km²) is made up of several
136 islands, the largest of which is *La Grande Terre* (17 000 km²). The Thio River catchment (397 km²) is
137 located on the east coast of this island (Figure 1-a). It has a mountainous relief, with an average
138 altitude of 416 m above sea level (i.e. minimum: 0 m, maximum: 1392 m, Figure 1-a) and an average
139 slope of 45%. Two dominant lithologies are present in the catchment: volcano-sedimentary
140 formations mainly located on the western part of the catchment and peridotite massifs concentrated
141 in the eastern part of the catchment. Cherts (22 %), sandstone (9 %), a mix of basalt, dolerite and
142 gabbro (6 %), polymetamorphic rocks (6 %) mainly constitute volcano-sedimentary formations
143 whereas peridotite massifs are composed of laterites (18 %), peridotites (17 %), serpentines (10 %)
144 and hazburgites (1 %) (Garcin et al., 2017) (Figure 1-b). The Thio River catchment is covered on 96%
145 of its surface by permanent vegetation. According to the mining registry, active and abandoned
146 mining sites and exploration cover 21 % of the catchment area (Figure 1-c).



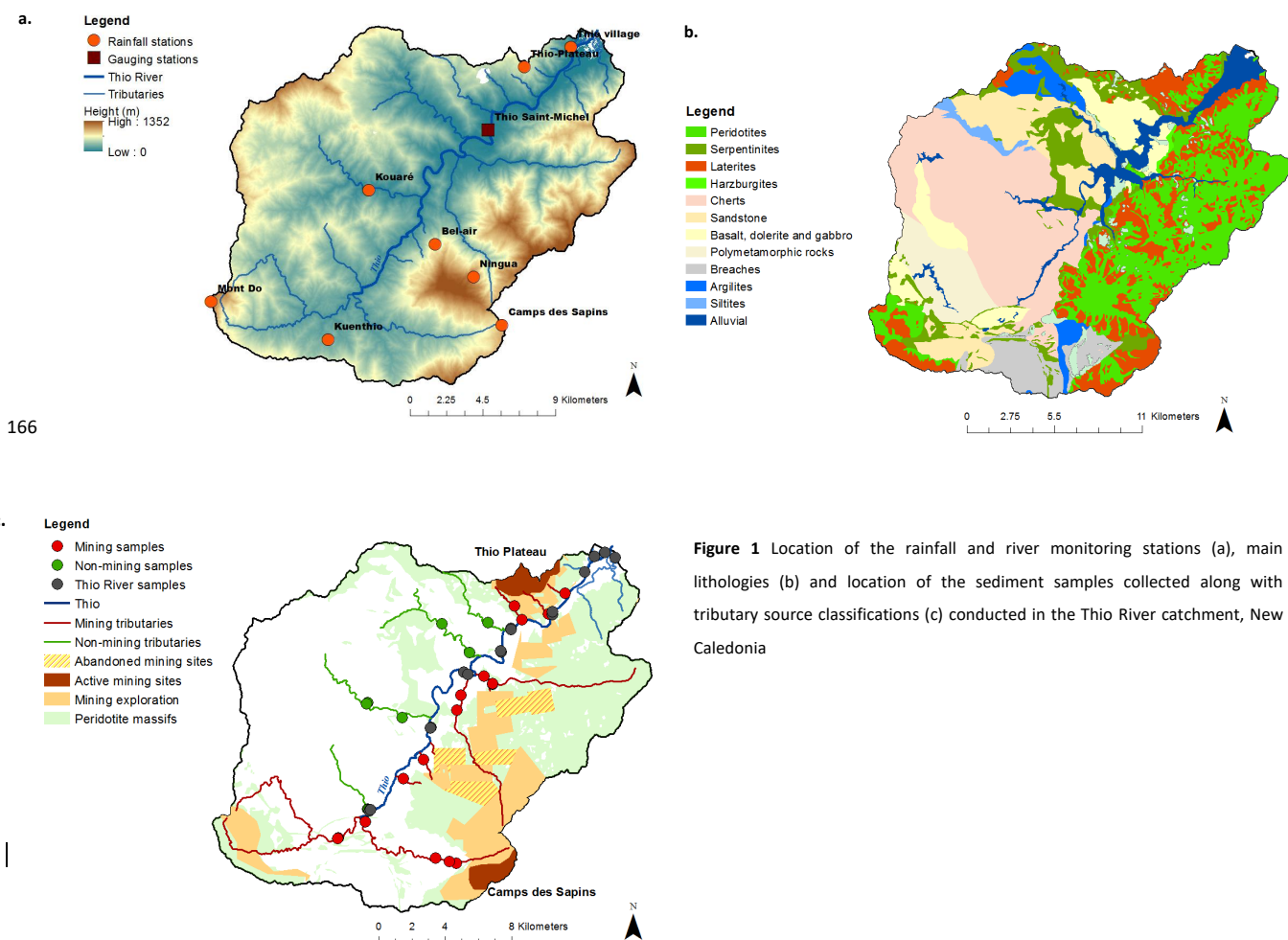
147 The Thio River catchment is subject to a tropical climate characterized by the alternation of a
148 hot wet season (November-April; mean temperature of 27 °C) and a cooler dry season (May-October;
149 mean temperature of 20 °C). The mean annual rainfall in the Thio River catchment is 1620 mm
150 despite strong seasonal fluctuations with the highest levels of precipitation recorded during the
151 cyclonic season between January and March (700 mm, 1981-2008; Alric (2009)). Although they only
152 occur on average once every 2.7 years, cyclones or tropical depressions may supply more than 20 %
153 of the annual rainfall in only one day according to local meteorological records (Météo France).

154

155 Twelve major tributaries flow into the main stem of the Thio River (28 km long) (Figure 1-b).
156 Ninety-two percent of the river channel length are characterized with slopes lower than 5 %.
157 According to Surell's classification (1841), the Thio River can be considered as torrential except in its
158 estuarine section. In addition, the extensive bare soil surface associated with past mining activities
159 (~10 sites), ongoing mining operations (e.g. 2 sites: Thio Plateau, Camps des Sapins) and the
160 occurrence of 6 km² of mining roads exacerbate runoff production as they contribute to increased
161 river network connectivity (Alric, 2009). This generates extensive erosion processes that are evident
162 across the entire Thio catchment with the widespread occurrence of rills, gullies, landslides and
163 channel bank erosion (Danloux and Laganier, 1991).

164

165



166

Figure 1 Location of the rainfall and river monitoring stations (a), main lithologies (b) and location of the sediment samples collected along with tributary source classifications (c) conducted in the Thio River catchment, New Caledonia



169 **1.2.Hydro-sedimentary monitoring**

170 Three rainfall stations (Thio Plateau, Thio village, Camps des Sapins; Figure 1-b) are operated
171 by Météo France and five others are managed by the DAVAR (Direction des Affaires Vétérinaires
172 Alimentaires et Rurales; i.e. Kouaré, Bel-Air, Ningua, Kuenthio, Mont Do), with daily records available
173 since 1952 for some stations (e.g. Thio village). Daily discharge has been monitored at a river gauging
174 station located on the main stem of the Thio River (at Saint-Michel) since 1981 by the DAVAR (Figure
175 1-a).

176 **1.3.Sources and river sediment sampling**

177 To trace the origin of sediment, lag deposits were collected as an alternative of suspended
178 sediment sampling on channel bars of mining tributaries (n= 16), non-mining tributaries (n= 8) and
179 the Thio River (n= 19) according to the tributary approach recommended by Lacey et al. (2017)
180 (Figure 1-c). They were sampled after two major floods (~10 year return period): (1) the tropical
181 depression of February 25, 2015 (n= 31) and (2) Cyclone Cook on April 10, 2017, (n= 12). These two
182 sample sets were respectively sampled between April 30 and May 5, 2015 and between May 16 and
183 17, 2017. At each sampling site, five to ten subsamples of fine sediment were collected across a 10
184 m² surface with a plastic trowel at exposed subaerial sites free of vegetation on channel bars. The
185 subsamples were composited into one sample representative of the fine sediment deposited on the
186 channel bars. The samples were oven-dried at 40°C for ~48 hours and sieved to 63 µm.

187 **1.4.Preparation of artificial mixture samples**

188 Equal quantities of all mining source samples (n= 16) were collected and mixed together to
189 create a composite sample of mining sources. The same process was carried out with non-mining
190 source samples (n= 8). The two composite samples respectively corresponding to mining and non-
191 mining sources were then mixed in known proportions to create artificial mixture samples (n= 21, 0-
192 100 % with a 5 % step, Table 1).



193 **Table 1** Proportions of mining and non-mining sources (%) in artificial mixture samples (M_i). M_6 was
194 *withdrawn from this study because an error occurred at the time of its completion (out of study).*

M_i	Proportions of mining sources (%)	Proportions of non-mining sources (%)
M1	0	100
M2	5	95
M3	10	90
M4	15	85
M5	20	80
M6	<i>25 (out of study)</i>	<i>75 (out of study)</i>
M7	30	70
M8	35	65
M9	40	60
M10	45	55
M11	50	50
M12	55	45
M13	60	40
M14	65	35
M15	70	30
M16	75	25
M17	80	20
M18	85	15
M19	90	10
M20	95	5
M21	100	0

195

196 **1.5.Source, river sediment and artificial mixture sample analyses**

197 A portable diffuse reflectance spectrophotometer (Konica Minolta 2600d) was used to
198 measure the spectra in the visible (365-735 nm with a 10-nm resolution, 39-wavelength class) on
199 Thio River sediment ($n= 19$), tributary source ($n= 16$) and artificial mixture samples ($n= 20$). Sample
200 quantities between 0.1 g and 4 g were stored in 60 mL polystyrene tubes and analyzed at the Institut
201 des Géosciences de l'Environnement (IGE, Grenoble, France). Because of the rather small measuring
202 area (i.e. 3-mm radius circle), and to take into account the possible heterogeneity within the
203 samples, three measurements were carried out on river sediment and sources samples. For artificial
204 mixture samples, the experimenter who conducted the analyses carried out four measurements.
205 Several parameters (i.e. D65 illuminant, 10° angle observer and specular component excluded) were



206 applied for each measurement. Raw data collected corresponds to the spectral reflectance
207 percentage for each of the 39-wavelength class. From these raw data, 15 variables of various
208 colorimetry models were derived. Among these components, XYZ tri-stimulus values were calculated
209 based on the colour-matching functions defined by the International Commission on Illumination (CIE
210 1931). The standardized tri-stimuli were then converted into CIE Lab and CIE Lu'v' cartesian coordinate
211 systems using the equations provided by CIE (1976) and then into CIE Lch, CIE L*a*b* cartesian
212 coordinate systems using the equations provided by CIE (1994) (Rossel et al., 2006). First Derivative
213 reflectance of the Visible Spectra (FDVS) of each sample was also derived from the initial reflectance
214 spectrum. According to Tiecher et al. (2015), the use of FDVS avoids differences in baseline positions
215 and to get rid of the small differences due to uncontrolled sources of variation, as sample packaging.

216 Measurements of 11 geochemical elements (i.e. Mg, Al, Si, K, Ca, Ti, Cr, Mn, Fe, Ni and Zn) on
217 the samples were conducted by pre-calibrated energy dispersive X-ray fluorescence spectrometry
218 (Epsilon 3, Malvern PANalytical) with certified reference samples including Internal Atomic Energy
219 Agency (IAEA) standards ($r^2 = 0.90-0.99$, mean relative error: 9% ,SD 8 %, minimum: 1%, maximum:
220 23%). Between 0.2 and 0.5 g of the samples were packed in small mass holder (SMH) cells with an air
221 double X-ray Mylar film and analyzed at the Laboratoire des Sciences du Climat et de
222 l'Environnement (LSCE, Gif-sur-Yvette, France). Samples were irradiated with a primary beam
223 generated by an Rh anode X-ray tube emitting electromagnetic waves between 100eV and 1MeV
224 with a maximum power, typical current and voltage fixed to 15 W, 3mA and 50 kV respectively. The
225 associated Si-drift detector had a Be window thickness of 8 μm and recorded the sample spectrum in
226 a 2D optical geometry configuration. X-ray intensities were converted into concentrations using the
227 Epsilon 3 software program through the application of the fundamental parameters method.



228 1.6. Statistical analysis and sediment tracing

229 1.6.1. Conventional mixing model

230 In general, the sediment source fingerprinting approach is composed of four main steps: (1)
231 range test, (2) the Mann-Whitney U test, (3) a stepwise discriminant function analysis and (4) a
232 mixing model (Collins et al., 1996). For the range test, all variables exhibiting values in the river
233 sediment samples that were outside of the range found in the potential sources (i.e. between the
234 minimum and maximum values found in source samples) were excluded from the analysis. It is
235 important to restrict the tracing parameters to those that show a conservative behavior to avoid
236 incorrect source prediction and consequently inaccurate estimations of source contributions (Sherriff
237 et al., 2015). Thereafter, the Mann-Whitney U test ($\alpha = 0.05$, p-value < 0.01) was performed to
238 evaluate whether remaining variables could discriminate the source samples. A stepwise
239 discriminant function analysis (DFA) was independently run on three set of potential tracing
240 properties: (1) colour parameters (i.e. 'colour'), (2) geochemical properties (i.e. 'geochemistry') and
241 (3) colour parameters and geochemical properties (i.e. 'colour + geochemistry'). For the last set, the
242 raw values of the variables were normalized in order to make them comparable. Indeed, several
243 colour parameters were within an order of magnitude of around 0.01 whereas for the geochemical
244 parameters the difference was around 10^6 mg kg^{-1} which resulted in a poorly conditioned matrix for
245 the DFA.

246 The following calculation was therefore applied on the variable values to normalize them: $x_i -$
247 $x_{\min} / x_{\max} - x_{\min}$ where x_i was value found in source sample (i), x_{\min} and x_{\max} were respectively the
248 minimum and maximum values found in the source samples. The DFA was carried out to select the
249 optimal number of potential tracers to discriminate the sources for each modelling approach with
250 the optimal number of potential tracers which must provide the lowest Wilks' lambda value from
251 analysis of variance. Indeed, the closer the Wilks' lambda value is to 1, the lower the variability within



252 the sources compared to the total variability. The DFA was performed in the backward mode with a p
253 >0.01 used to select a tracer and p <0.01 used to remove a tracer.

254 Finally, a classical solver-based mixing model was used to model the source contributions from
255 the mining and non-mining tributaries to target sediment through simultaneously minimizing the
256 mixing model difference (MMD) (Evrard et al., 2019):

$$257 \quad MMD = \sum_{i=1}^n ((C_i - (A_i x + B_i(1 - x)))/C_i) \quad \text{Equation 1}$$

258 where n is the number of parameters in the model chosen by the selection process (i.e. steps 1, 2, 3);
259 C_i is the Thio River sediment sample parameter (i); x and (1-x) were respectively the contributions of
260 source A and B (i.e. mining and non-mining tributaries); A_i is the mean of parameter (i) in source A
261 and B_i is the mean of parameter (i) in source B. The proportional contribution from each source (x)
262 was modelled by solving Equation 1 with the Solver Function in Microsoft Excel with x being between
263 0 and 1 and the sum of source contributions (i.e. x and 1-x) equaling 1. The GRG Non-Linear solving
264 method was used with automatic scaling in Solver, ignoring integer constraints, with a maximum run
265 time of 5000 and allowing for 2500 iterations. A multi-start population size of 2500 was used along
266 with the same random seed for each of the model runs while requiring bounds on the variables. A
267 constraint precision and convergence of $1.0 \cdot 10^{-6}$ were selected. To test the reliability of the 'colour',
268 'geochemistry' and 'colour + geochemistry' models, these latter were tested on artificial mixture
269 samples.

270 1.6.2.FDVS- PLSR model

271 FDVS-PLSR models were built following the methodology described in Poulenard et al. (2012).
272 The first step consisted in applying a principal component analysis (PCA) to evaluate the overall
273 variability between FDVS (i.e. 38 wavelengths) of source samples. Subsequently, a discriminant
274 analysis (DA) was conducted based on the PCA scores. The purpose of this analysis was to compare
275 the Mahalanobis distance between sources samples and to determine if FDVS of source samples

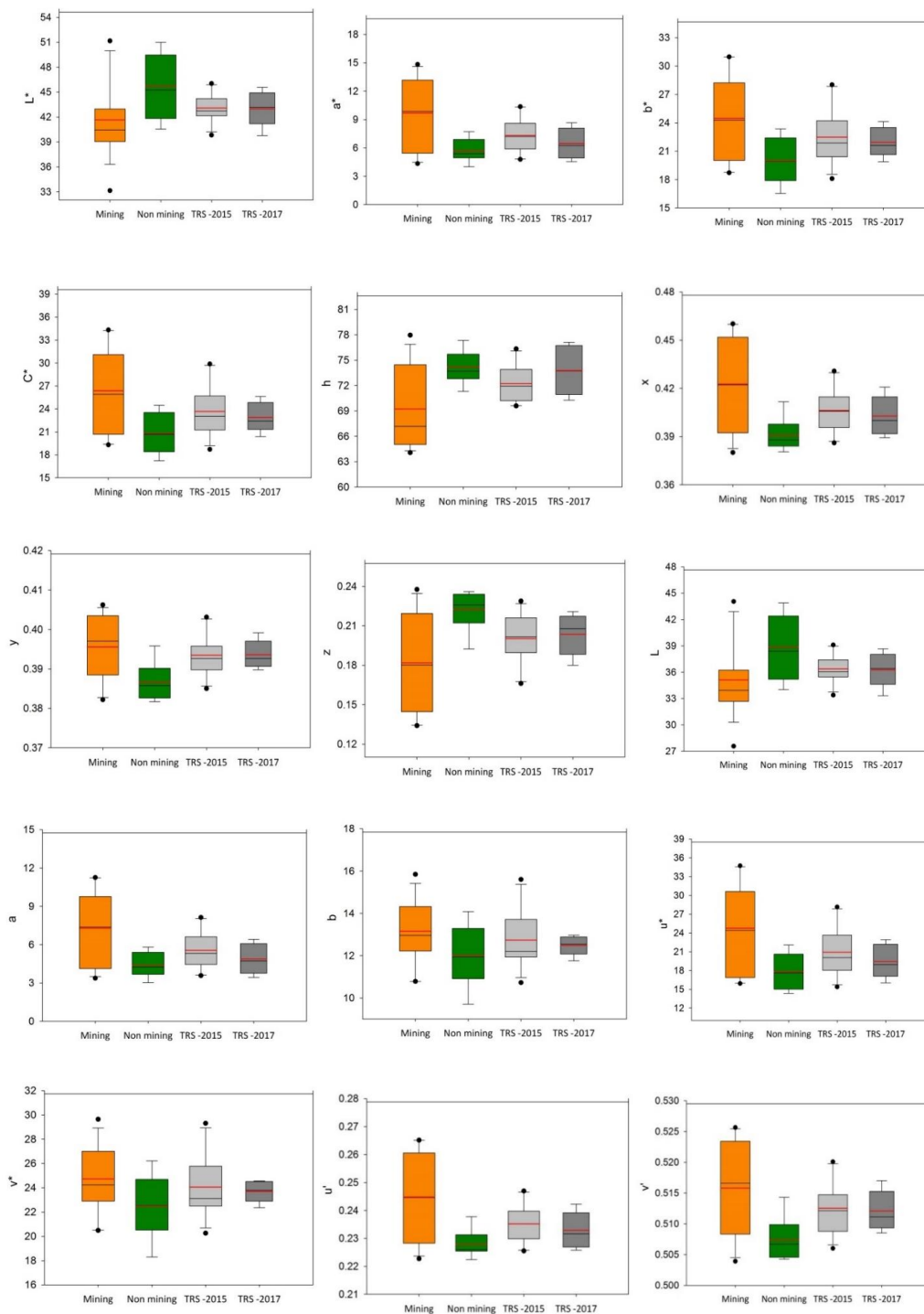


276 could discriminate the sources. Relationships between FDVS (x variate) and the corresponding weight
277 contribution of the sediment source data sets (y variate) were analyzed using PLSR. The PLSR models
278 were carried out based on the component set providing the lowest predictive error (PRESS, option on
279 XLStat software). Two independent PLSR models were built to estimate the two sediment source
280 contributions. As the artificial mixtures were measured four times by spectroscopy, 84 FDVS of
281 artificial mixture samples were generated including 50 values that were randomly selected to build
282 the models (training set (ST)) and 34 to validate the models (validation set (SV)). The SV:ST ratio used
283 was approximately 1:2, which is in agreement with recommendations provided in the literature
284 (Daszykowski et al., 2002). To evaluate the performance of PLSR models, several indicators such as
285 coefficient of linear regression (r^2), root mean square error of calibration (RMSEC) and root mean
286 square error of prediction (RMSEP) values were calculated. Unlike the conventional fingerprinting
287 approach, the estimated contributions of sources were not limited to be in the range of 0 % and 100
288 %. In a similar way, the sum of source contributions was not constrained to be equal to 100 %. As a
289 result, another way to control the reliability of predictions was to sum the prediction proportions of
290 both models (Legout et al., 2013). FDVS of river sediment samples were then introduced into these
291 PLSR models to estimate the contribution of sediment sources.

292 Results

293 **1.7.Source description**

294 The ranges of values of all colour parameters measured in the Thio River sediment samples
295 systematically plotted within the range of values observed in the two potential sources (i.e. mining
296 and non-mining tributaries; Figure 2 and Table 2). The range test results confirmed the conservative
297 character of these parameters. For geochemical properties, elemental concentrations measured in
298 the river sediment also plotted within the range of concentrations found in sources (Sellier et al.,
299 2019). According to the range test results, all properties were determined to be conservative.



300 **Figure 2** Box-plots of colour parameter values in the <63 μm fraction of sediment collected on the mining
 301 tributaries (Mining), non-mining tributaries (Non-mining) and the main Thio River (Thio River sediment (TRS)-
 302 flood events of 2015 and 2017). The box indicates the location of the first and third quartiles; the black line
 303 indicates the median value; the red line indicates the mean value



304 **Table 2** Geochemical element content and colour parameter values in the <63 µm fraction of sediment sources
 305 and Thio River sediment; results of Mann-Whitney U test and individual DA used to identify the potential
 306 tracers to differentiate sources supplying sediment to the Thio River

Fingerprinting property	Mann-Whitney U test		DA- correctly classified samples (%)	Mining tributaries (n= 16)	Non-mining tributaries (n= 8)	Thio River sediment 2015 (n= 11)	Thio River sediment 2017 (n= 8)
	U-value	p-value					
<i>Geochemical tracers</i>							
Al ($g\ kg^{-1}$)	8	0.000	87.5	21 ± 21	67 ± 8	43 ± 15	29 ± 6
Ca ($mg\ kg^{-1}$)	21	0.007	62.5	3731 ± 470	9286 ± 5194	5281 ± 1201	3945 ± 666
Cr ($mg\ kg^{-1}$)	124	< 0.0001	83.3	7480 ± 4606	706 ± 967	4359 ± 2185	5715 ± 1786
Fe ($g\ kg^{-1}$)	121	0.000	91.6	144 ± 70	62 ± 24	43 ± 15	29 ± 6
K ($mg\ kg^{-1}$)	2	< 0.0001	95.8	1657 ± 2160	14019 ± 3702	5944 ± 3294	3750 ± 974
Mg ($g\ kg^{-1}$)	119	0.000	83.3	99 ± 59	16 ± 13	88 ± 33	117 ± 21
Mn ($mg\ kg^{-1}$)	108	0.006	83.3	2531 ± 1317	1439 ± 606	2068 ± 667	1786 ± 516
Ni ($mg\ kg^{-1}$)	125	< 0.0001	91.6	6576 ± 5075	358 ± 339	4218 ± 1938	4341 ± 1239
Si ($g\ kg^{-1}$)	6	< 0.0001	91.6	178 ± 42	254 ± 28	221 ± 15	204 ± 7
Ti ($mg\ kg^{-1}$)	13	0.001	87.5	1409 ± 2077	5446 ± 835	2771 ± 1197	1663 ± 457
Zn ($mg\ kg^{-1}$)	68	0.834	-	146 ± 47	125 ± 4	134 ± 17	125 ± 8
<i>Colour parameters</i>							
L*	24	0.013	-	41.6 ± 4.6	45.7 ± 3.9	43.1 ± 1.7	43.0 ± 2.0
a*	104	0.013	-	9.7 ± 3.8	5.7 ± 1.2	7.3 ± 1.9	6.5 ± 1.7
b*	106	0.009	70.8	24.5 ± 4.5	20.0 ± 2.5	22.5 ± 3.0	21.9 ± 1.6
C*	108	0.006	66.6	26.4 ± 5.5	20.8 ± 2.7	23.7 ± 3.5	22.9 ± 2.0
h	26	0.019	-	69.2 ± 4.8	74.2 ± 1.9	72.2 ± 2.2	73.8 ± 2.9
x	107	0.007	75	0.42 ± 0.03	0.39 ± 0.01	0.41 ± 0.01	0.40 ± 0.01
y	111	0.003	79.2	0.396 ± 0.008	0.387 ± 0.005	0.393 ± 0.005	0.394 ± 0.004
z	19	0.005	75	0.18 ± 0.04	0.22 ± 0.01	0.20 ± 0.02	0.20 ± 0.02
L	27	0.013	-	35.1 ± 4.2	38.9 ± 3.7	36.4 ± 1.6	36.3 ± 1.9
a	103	0.016	-	7.3 ± 2.9	4.4 ± 1.0	5.6 ± 1.5	4.9 ± 1.2
b	91	0.106	-	13.1 ± 1.5	12.0 ± 1.5	12.7 ± 1.4	12.5 ± 0.4
u*	101	0.023	-	24.8 ± 6.9	17.8 ± 2.8	20.9 ± 4.0	19.4 ± 2.7
v*	93	0.081	-	24.7 ± 2.8	22.5 ± 2.7	24.1 ± 2.6	23.7 ± 0.8
u'	105	0.011	-	0.245 ± 0.016	0.228 ± 0.005	0.235 ± 0.007	0.233 ± 0.007
v'	111	0.003	79.2	0.516 ± 0.008	0.507 ± 0.004	0.513 ± 0.004	0.512 ± 0.003

307



308 **1.8.Selection of parameters/properties for modelling**

309 1.8.1. 'Colour' model

310 According to the Mann-Whitney U test results, six colour parameters (*i.e.* b^* , C^* , x , y , z , v')
311 provided significant discrimination between the two sediment sources (*i.e.* p -value < 0.01 , Table 2).
312 The backward DFA selected only v' as the optimal tracer of mining and non-mining source sediments
313 (Figure 2, Table 3). Although this parameter correctly classified 79.2 % of sources, the high Wilk's
314 lambda value obtained (*i.e.* 0.7209, Table 3) induced that only 27.9 % of variance was explained by v' .
315 The low Mahalanobis distance value obtained (*i.e.* 1.6) confirmed that sediment sources were not
316 well separated. Accordingly, and owing to the high error percentage of the source discrimination
317 provided by this approach (*i.e.* 72.1 %), source contributions were not modeled with the 'colour'
318 model.

319 1.8.2. 'Geochemistry' model

320 When considering the two potential sediment sources, all geochemical properties (except Zn)
321 were selected as potentially discriminant by the Mann-Whitney U test (*i.e.* p -value < 0.01 , Table 2).
322 Among the 10 potential tracers, K was selected by the backward DFA to model sediment source
323 contributions from mining and non-mining tributaries with 95.3 % of sources correctly classified and
324 83.1 % of variance explained by K. This percentage of variance explained was deduced from the final
325 Wilk's lambda value obtained (*i.e.* 0.1691). Moreover, the Mahalanobis distance value showed that
326 the sediment sources were well separated from each other with a significant distance of 20.3 (Table
327 3) (Sellier et al., 2019).

328 1.8.3. 'Colour + geochemistry' model

329 When combining colour parameters and geochemical properties, the DFA selected five optimal
330 tracers (*i.e.* K, Ca, Ti, b^* , C^*) able to correctly classify 100 % of the sources. A significant improvement
331 in the source discrimination was observed with the lowest Wilk's lambda value obtained (*i.e.* 0.0734)
332 and the highest percentage of variance explained (*i.e.* 92.6 %). Moreover, the Mahalanobis distance



333 value obtained (i.e. 52.1) was more than 2.5 times higher than that estimated with the
334 'geochemistry' model (Table 3), thus resulting in a better separation between sediment sources than
335 the previous approach (i.e. 'geochemistry')

336 **Table 3** Results of DFA used to identify the optimum tracer combination to differentiate sources supplying
337 sediment to the Thio River

Fingerprint property selected	Wilks' Lambda	Variance explained by the variables (%)	Squared Mahalanobis distance	Correctly classified samples (%)
<hr/>				
'Colour'				
v'	0.7209	27.9	1.6	79.2
<hr/>				
'Geochemistry'				
K	0.1691	83.1	20.3	95.3
<hr/>				
'Colour + Geochemistry'				
K, Ca, Ti, b*, C*	0.0734	92.6	52.1	100

338

339 1.9. Assessment of model performance on artificial mixture samples

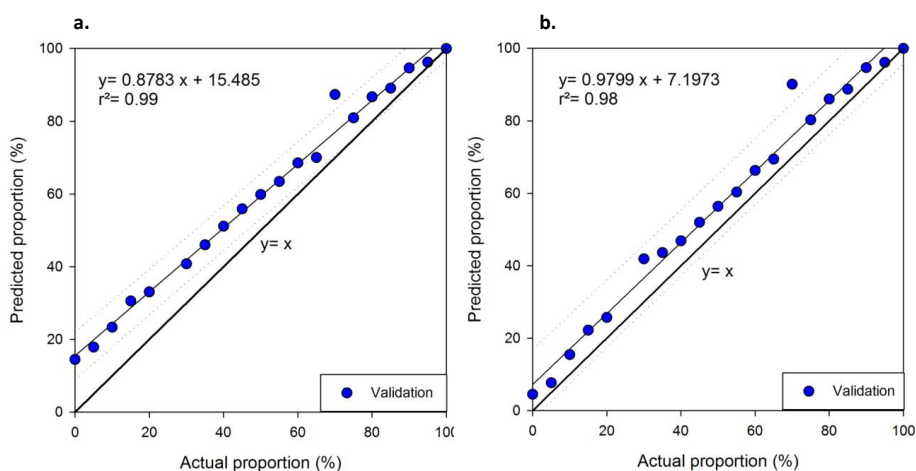
340 Prior to applying mixing models to river sediments, preliminary tests were conducted to
341 control the validity of the models (i.e. 'geochemistry' and 'colour + geochemistry') and the associated
342 estimations of source contribution errors. When applying these models on the artificial mixture
343 samples, actual and predicted proportions were well correlated for both models (i.e. $r^2 = 0.99$ and $r^2 =$
344 0.98 respectively for 'geochemistry' and 'colour + geochemistry' models) (Figure 3).

345 However, the 'geochemistry' model described in Figure 3-a showed that the contributions of
346 mining tributaries were overestimated. With 100 % of actual mining contributions, 100 % of mining
347 contribution was predicted by the model. However, instead of 0 % of actual mining contributions, a
348 mining contribution of 15.5% was predicted by the model. It means that the more the estimated
349 mining source contributions tends towards 0%, the greater the associated overestimation (i.e.
350 maximum 15.5 %) (Figure 3-a). The 'colour + geochemistry' model also provided a slight



351 overestimation of the contribution of mining tributaries (i.e. 7 % intercept of the regression line,
352 Figure 3-b). Given the slope of the regression line calculated is close to 1 (i.e. 0.98), this 7%
353 overestimation remains constant over the entire range of potential contributions.

354 **Figure 3** Comparison between actual mining source proportions prepared in artificial mixtures and the mining



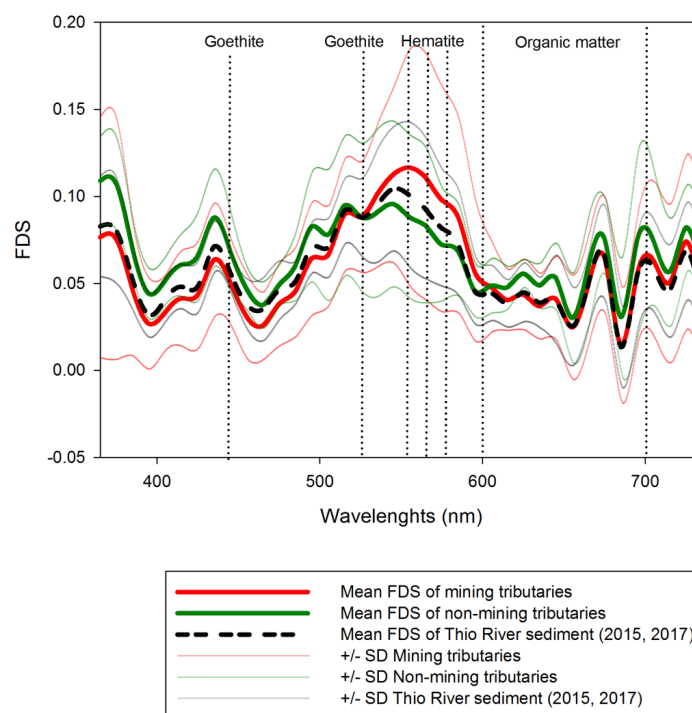
355 source proportions predicted by the 'geochemistry' (a) and 'colour + geochemistry' (b) models

356 1.10. Building partial least-squares models based on FDVS

357 Mining sources are characterized by a red-orange color while sediments originating from non-
358 mining sources are grey. The color contrasts may be explained by the distinct geochemical
359 composition of these sources. Mean FDVS indicated the presence of goethite (i.e. at 445 and 525
360 nm), hematite (i.e. at 555, 565 and 575 nm), and organic matter (i.e. between 600-700 nm) (Debret
361 et al., 2011) in both mining and non-mining sources (Figure 4). In similar way, the Thio River sediment
362 samples (2015, 2017) showed similar characteristics since the variations of the mean FDVS remained
363 between those found in the sources (Figure 4). Nevertheless, some differences can be observed
364 between the sources. The spectral signature of goethite is slightly stronger at 445 nm in non-mining
365 tributaries compared to mining tributaries. No difference between sources was observed at 525 nm,
366 the second wavelengths characterizing the presence of goethite. In contrast, the spectral signature of



367 hematite (*i.e.* at 555, 565 and 575 nm) was stronger in mining tributaries than in non-mining
368 tributaries.

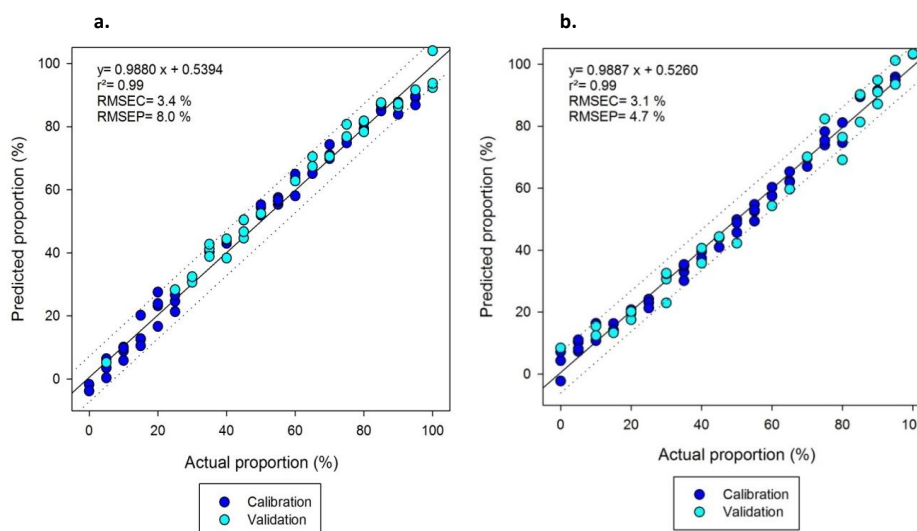


369 **Figure 4** FDVS measured in the <63 μm fraction of sources and Thio River sediment samples

370 To test the potential discrimination offered by FDVS, a PCA was applied on the source data set.
371 The first ten principal components from PCA explained 99 % of the total variation in the spectra. The
372 DFA performed on these components resulted in a final Wilks' lambda value of 0.1585. It means that
373 84.1 % of variance is explained by these ten components. Moreover, 100 % of the source samples
374 were correctly classified. The performances of FDVS-PLSR models are presented in Figure 5. The
375 mining and non-mining tributary FDVS-PLSR models provided an excellent correlation between actual
376 and predicted proportions with r^2 and slopes close to 1 and intercepts of linear regression close to 0.
377 The root mean square error of calibration (RMSEC) values estimated for both models were low, *i.e.*
378 3.4 % and 3.1 % respectively for mining and non-mining tributary models. These models also



379 provided a good predictability of source contributions with low root mean square error of prediction
380 (RMSEP) values (i.e. 8.0 % and 4.7 % respectively for mining and non-mining tributary models).
381 Another way to control the reliability of predictions was to sum the predicted proportions of both
382 models (Legout et al., 2013). Considering the whole data set used in the construction of the partial
383 least-squares regression models (i.e. calibration and validation) led to a mean sum of the predicted
384 source proportions of 102 % (SD 3 %, range: 98-114 %), thus highlighting the effective prediction
385 performance of FDVS-PLSR models.



386 **Figure 5** Building of FDSV-PLSR models for mining sources (a) and non-mining sources (b)

387 1.11. Source apportionment modelling

388 1.11.1. 'Geochemistry' model

389 The 'geochemistry' model estimated that the mining tributaries contributed an average of 65
390 % (SD 27 %) of the Thio River sediment during the 2015 flood event; they therefore dominated
391 sediment inputs overall during this event. Nevertheless, non-mining tributaries locally and mainly
392 contributed to the sediment inputs at three sampling points along the Thio River (Figure 6-a, Table 4,
393 sampling points [3, 5, 7]). These contributions did not, however, compensate those provided by

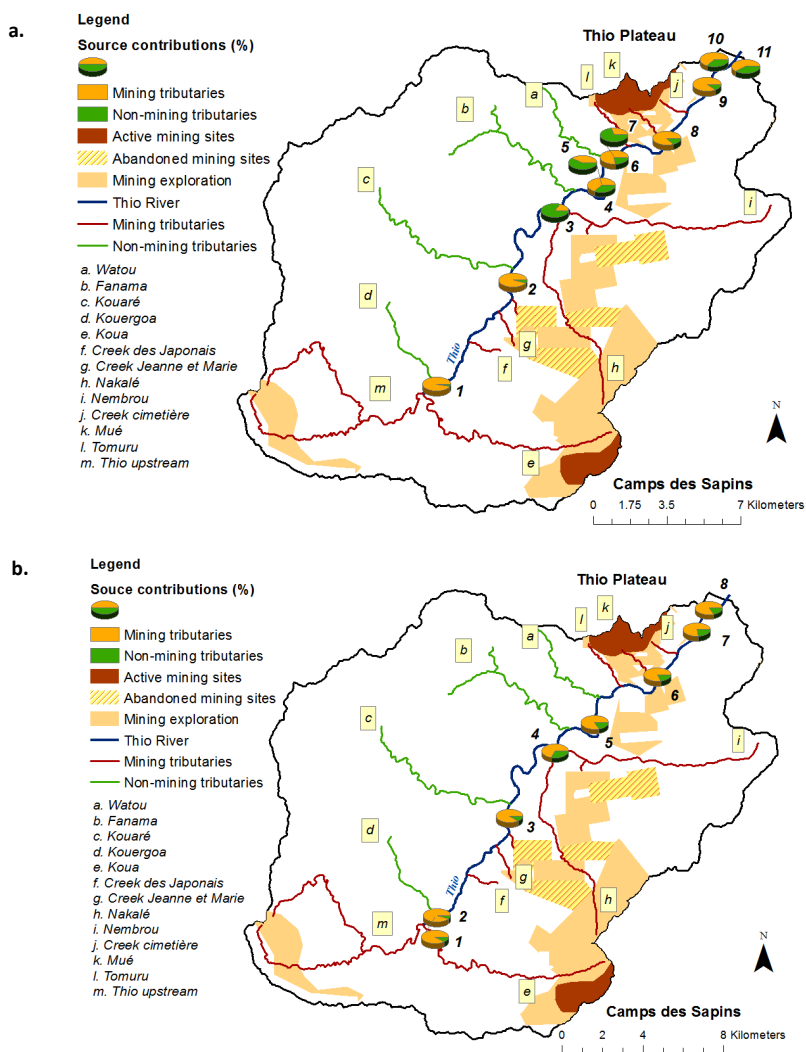


394 mining tributaries in the estuary (63-89 %). Indeed, the dominant mining contributions found in
395 upstream river reaches (96 %, Figure 6-a, Table 4, sampling point [1]) gradually decreased along the
396 Thio River, fluctuating between 17-77 % before increasing again at the confluence between the Thio
397 River and the mining tributaries draining the Thio Plateau mining area (i.e. 85 %, Figure 6-a, Table 4,
398 sampling point [8]) and reaching 60-64 %.

399

400 This model also demonstrated that mining tributaries dominated sediment inputs with a mean
401 contribution of 83 % (SD 8%) during the 2017 flood event (Table 5). The lowest mining tributary
402 contributions estimated (i.e. 69 %) was found after the confluence with the Kouaré non-mining
403 tributary (Figure 6-b, Table 5, sampling point [4]). Nevertheless, further downstream, the proportions
404 of the mining sources increased again to reach 77-83 % in the estuary (Figure 6-b, Table 5, sampling
405 points [7, 8]).

406



407 **Figure 6** Relative contributions of mining and non-mining tributaries to the sediment collected in the Thio River
 408 during the 2015 (a) and 2017 (b) flood events using the 'geochemistry' model

409

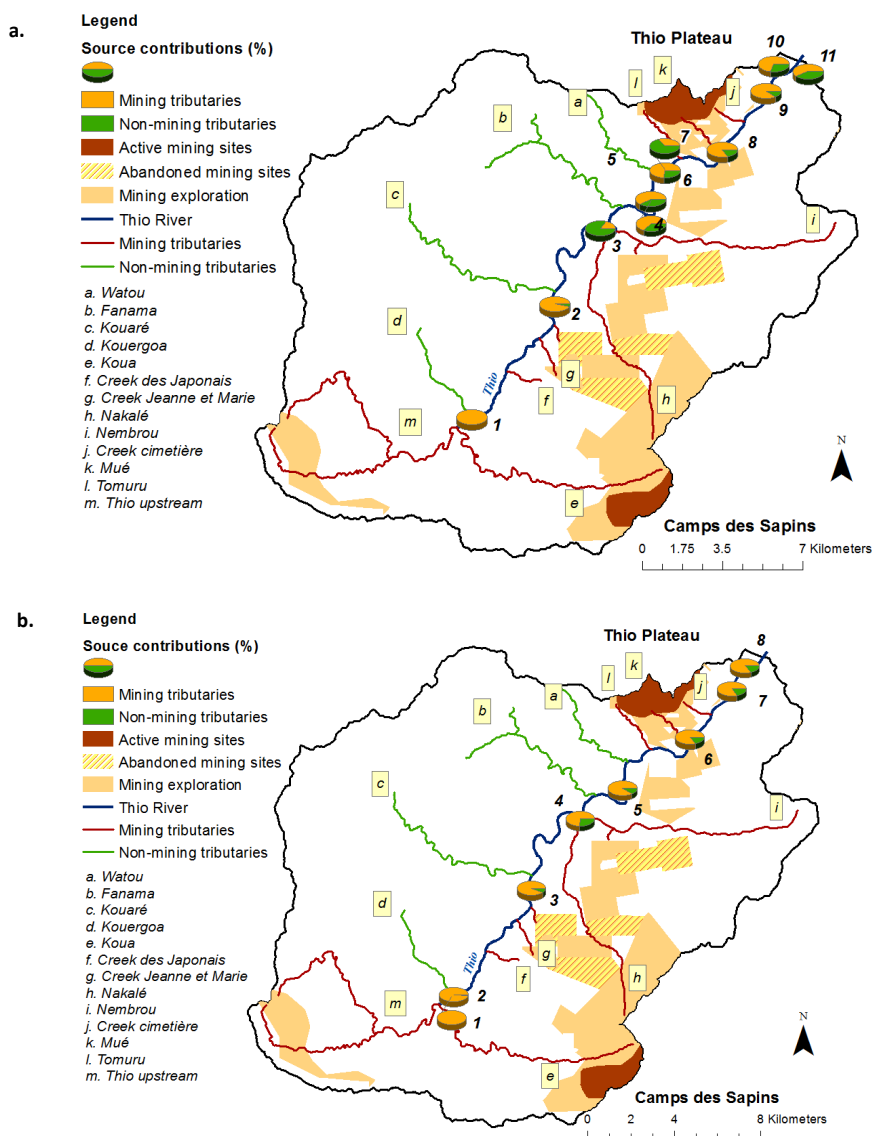


410 1.11.2. 'Colour + geochemistry' model

411 Similar results were obtained with the 'colour + geochemistry' model. The contributions of
412 mining tributaries were estimated to an average of 68 % (SD 25 %) for the 2015 flood event. Mining
413 tributary contributions provided almost all the sediment transiting the uppermost reach of the Thio
414 River (i.e. 99 %, Figure 7-a, Table 4, sampling point [1]). However, after the confluence with the
415 Kouaré tributary, non-mining tributaries dominated with a contribution of 83 % (Figure 7-a, Table 4,
416 sampling point [3]). Further downstream, the contribution of mining tributaries increased again with
417 supplies varying between 34- 89 % to reach 58- 70 % in the estuary (Figure 7-a, Table 4). The largest
418 difference between 'geochemistry' and 'colour + geochemistry' model outputs was 18 % for the 2015
419 flood event.

420 The 'colour + geochemistry' model also demonstrated that 88 % (SD 8 %) of the sediment
421 supply originated from mining tributaries during the 2017 flood event. Along the Thio River, mining
422 tributary contributions varied between 100 % in the uppermost reach, 74% after the Kouaré river
423 confluence and 83-85% in the estuary (Figure 7-b, Table 5). The largest difference between
424 'geochemistry' and 'colour + geochemistry' model outputs was 10 % for the 2017 flood event (Table
425 5).

426



427 **Figure 7** Relative contributions of mining and non-mining tributaries to the sediment collected in the Thio River
 428 during the 2015 (a) and 2017 (b) flood events using the 'colour + geochemistry' model



429 1.11.3.FDVS-PLSR model

430 When applying the FDVS-PLSR models (i.e. mining and non-mining tributary contributions) to
431 the river sediment samples (2015, 2017), the mean sums of the source contributions were 92 % (SD 8
432 %) and 80 % (SD 13 %), respectively, for the 2015 and 2017 flood events (Tables 4 and 5). Owing that
433 predicted sums were different from the expected 100%, a bar plot display of the source contributions
434 has been chosen to facilitate the interpretation of the results (Figure 8).

435 According to the FDVS-PLSR model results, 34 % (SD 22 %) of sediment supply originated from
436 mining tributaries while non-mining tributary contribution provided 58 % (SD 18 %) of the sediment
437 input for the 2015 flood event (Figure 8-a, Table 4). In the upper part of the Thio River catchment,
438 non-mining tributaries largely dominated with a contribution of 80 % versus 6 % for mining
439 tributaries. Along the Thio River, mining tributary contributions gradually increased to reach 70 %
440 after the Mué tributary confluence (i.e. one of tributaries draining the Thio Plateau Mine, Figure 8-a,
441 Table 4, sampling point [9]). The non-mining tributary contributions fluctuated along the Thio River
442 between 41-85 % (Figure 8-a, Table 4, sampling points [2-8]) and reached a minimum (i.e. 28 %,
443 Figure 8-a, Table 4, sampling point [9]) after the Mué tributary confluence. In the estuary, sediment
444 supply was originated from 51-70 % of mining tributaries and 28- 52 % of non-mining tributaries
445 (Figure 8-a, Table 4, sampling points [9, 10, 11]).

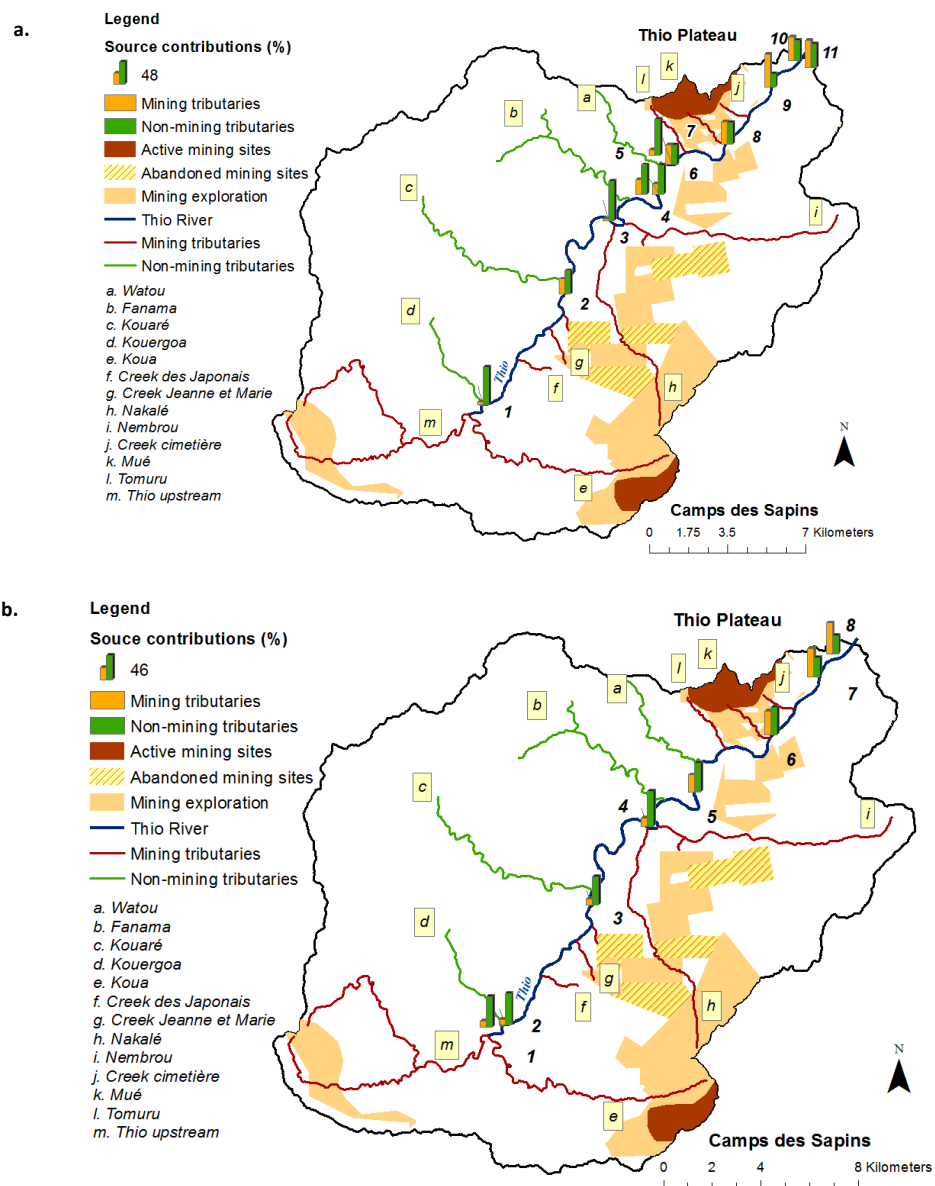
446 The FDVS-PLSR models also indicated that mining and non-mining tributaries respectively
447 contributed a mean of 29 % (SD 20 %) and 51 % (SD 11 %) of sediment (Figure 8-b, Table 5) during
448 the 2017 flood event. In a similar way, mining contributions gradually increased along the Thio River
449 from 11 % in upper parts to reach 52-58 % in the estuary. On the contrary, non-mining contributions
450 gradually decreased from 56 % in uppermost parts to reach 35-36 % in the estuary (Figure 8-b, Table
451 5).

452 In summary, the FDVS-PLSR models provided opposite results to those of the conventional
453 sediment fingerprinting approach (i.e. 'geochemistry' and 'colour + geochemistry' models). According



454 to the FDVS-PLSR models, non-mining tributaries contributed the majority of the sediment supply for
455 the 2015 (58 %, SD 18 %) and 2017 (51 %, SD 11 %) flood events. On the contrary, the 'geochemistry'
456 and 'colour + geochemistry' models demonstrated that mining tributary contributions dominated
457 sediment supply for the 2015 (i.e. respectively 65 % (SD 27%) and 68 % (SD 28 %)) and 2017 flood
458 events (i.e. respectively 83% (SD 8%) and 88 % (SD 8%)).

459



460 **Figure 8** Relative contributions of mining and non-mining tributaries to the sediment collected in the Thio River
 461 during the 2015 (a) and 2017 (b) flood events using the FDVS-PLSR models



462 **Table 4** Source contributions calculated by FDVS-PLSR, 'geochemistry', 'colour + geochemistry' approaches for sediment deposited during the flood of February 25,2015

Sampling point	Mining tributary contributions (%)			Non-mining tributary contributions (%)			Sum of source contributions (%)		
	FDS- PLSR	Geochemistry	Colour + Geochemistry	FDS- PLSR	Geochemistry	Colour + geochemistry	FDS- PLSR	Geochemistry	Colour + geochemistry
	1	6	96	99	80	4	1	86	100
2	33	95	96	51	5	4	84	100	100
3	4	17	17	85	83	83	90	100	100
4	32	65	65	64	35	35	96	100	100
5	22	41	59	63	59	41	85	100	100
6	42	77	74	41	23	26	83	100	100
7	12	29	34	79	71	66	91	100	100
8	47	85	83	46	15	17	93	100	100
9	70	88	89	28	12	11	98	100	100
10	51	64	70	44	36	30	94	100	100
11	59	60	58	52	40	42	111	100	100
M (%)	34	65	68	58	35	32	92	100	100
SD (%)	22	27	25	18	27	25	8	-	-
Minimum (%)	4	17	17	28	4	1	84	-	-
Maximum (%)	70	96	99	85	83	83	111	-	-

|



464 **Table 5** Source contributions calculated by FDVS-PLSR, 'geochemistry', 'colour + geochemistry' approaches for sediment deposited during the flood of April 10,2017

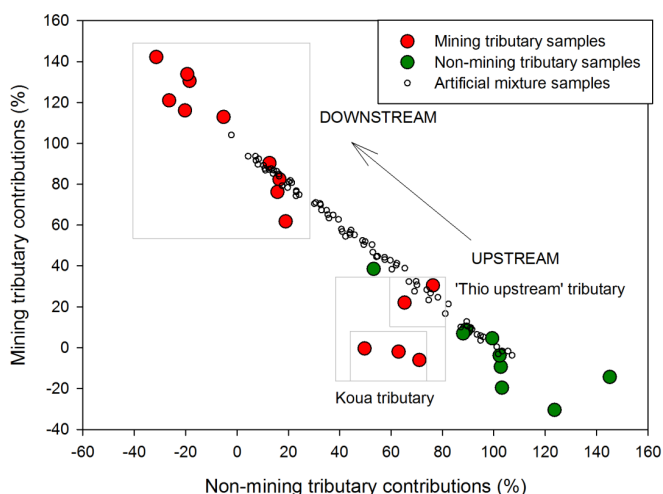
Sampling point	Mining tributary contributions (%)			Non-mining tributary contributions (%)			Sum of source contributions (%)		
	FDS- PLSR	Geochemistry	Colour + Geochemistry	FDS- PLSR	Geochemistry	Colour + geochemistry	FDS- PLSR	Geochemistry	Colour + geochemistry
1	11	90	100	56	10	0	66	100	100
2	9	94	98	58	6	2	68	100	100
3	11	89	92	52	11	8	63	100	100
4	16	69	74	66	31	26	82	100	100
5	32	82	89	54	18	11	86	100	100
6	44	81	84	51	19	16	95	100	100
7	52	77	83	36	23	17	88	100	100
8	58	83	85	35	17	15	92	100	100
M (%)	29	83	88	51	17	12	80	100	100
SD (%)	20	8	8	11	8	8	13	-	-
Minimum (%)	9	69	74	35	6	0	63	-	-
Maximum (%)	58	94	100	66	31	26	95	-	-

|



466 **1.6.Complementary tests: representativeness of artificial mixture samples used for the**
467 **FDVS-PLSR models compared to source samples**

468 Given the opposite results obtained in terms of source contributions between FDVS-PLSR
469 models on the one hand and 'geochemistry' and 'colour + geochemistry' models on the other hand,
470 complementary analyses were carried out on individual source samples (i.e. not the composite
471 samples used to create the artificial mixtures) to estimate their composition in terms of source
472 contributions with FDVS-PLSR models. As done in Legout et al. (2013) to assess uncertainties in the
473 fingerprinting approach due to source heterogeneity, they were considered as river sediment
474 samples. A mean sum of the predicted source proportions of 94 % (SD 17 %, range: 49-131 %) was
475 calculated from the source sample data set. The compositions of mining and non-mining tributary
476 samples in Figures 9 and 10 show that artificial mixture samples built from a mix between the
477 composite mining source sample and the composite non-mining source sample did not cover entirely
478 the range of values found in all the sources samples, which may explain why some source samples
479 showed mining and non-mining tributary composition lower than 0 and/or higher than 100 %.

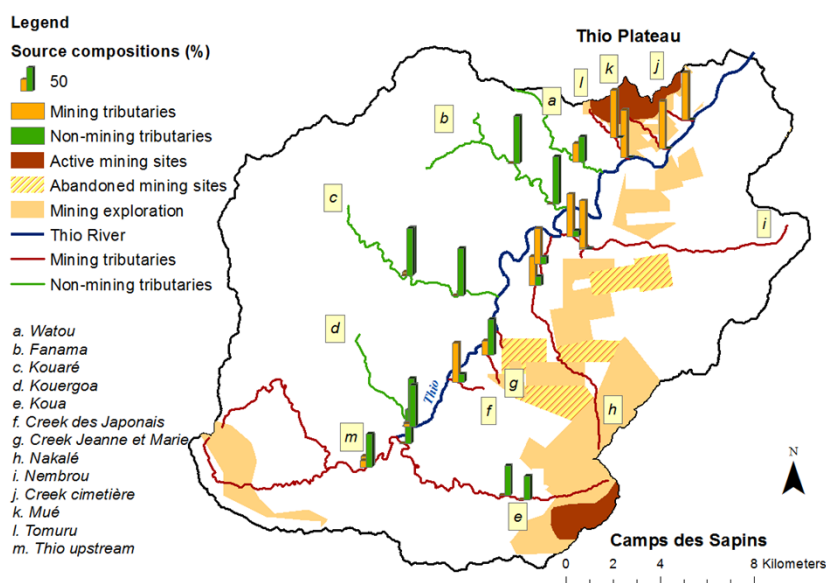


480

481 **Figure 9** Relative compositions of mining and non-mining sources estimated by the FDVS-PLSR models
482 applied to the individual source sediment samples



483 Moreover, two sub-groups of mining tributary samples can be distinguished, the first one
484 corresponding to samples collected on the mining tributaries located in the uppermost part of the
485 catchment and the second to samples collected on the mining tributaries located further
486 downstream. The FDVS-PLSR differentiated rather well the second group since the mining tributary
487 composition is dominant in these samples. On the contrary, the first group referred to as 'Upstream'
488 merged with the non-mining tributary samples (Figure 9). Indeed, Figure 10 shows the mining
489 tributaries located in the upper part of the catchment were defined as 'non-mining tributaries' by the
490 FDVS-PLSR model.

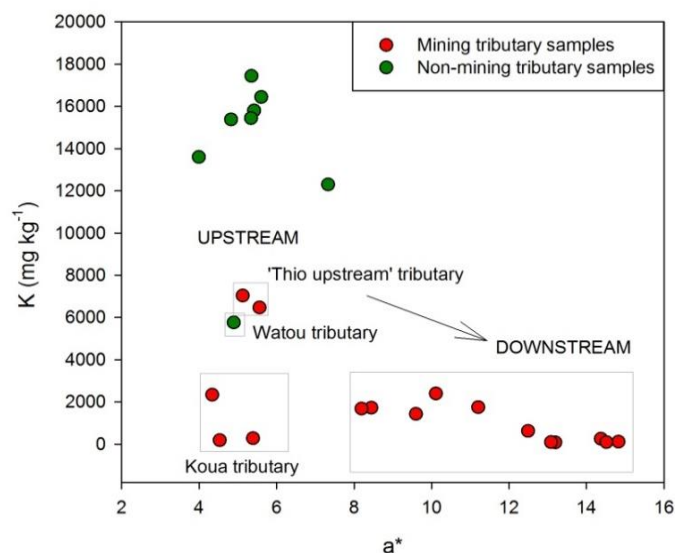


491 **Figure 10** Relative compositions of mining and non-mining sources estimated by the FDVS-PLSR models applied
492 to the individual sediment sources in the Thio River catchment

493 The low K contents found in these samples confirmed, however, that they were mainly
494 supplied by mining sources (Figure 11). Nevertheless, a colour difference could be observed visually
495 and through variations of the a^* parameter: the a^* values increased from upper parts to lower,
496 which results in an increasingly red coloration of mining tributary samples in downstream direction.
497 Figure 11 shows also that the a^* values found in samples collected in the upper catchment part



498 overlapped with those of non-mining tributary samples. Among the 'upstream' mining tributary
499 samples, only three samples collected on the Koua tributary (i.e. draining Camps des Sapins mine)
500 showed values that were not comprised in the ranges covered by the artificial mixture samples
501 (Figure 9).



502 **Figure 11** Diagram of K contents as a function of a* parameter values within sediment sources and artificial
503 mixture samples

504 Discussion

505 1.7. Advantages and limits of models

506 1.7.1. 'Colour' model

507 One of the objectives of this study was to test the contribution of spectrophotometry for
508 improving the source discrimination. Indeed, visual observations indicated that mining tributary
509 samples were red-orange whereas non-mining tributary samples were rather grey. However, the
510 results showed that the colour parameters, when used individually, did not provide sufficient
511 discrimination between sources (Table 2) to meet this objective. Indeed, some mining tributary
512 samples showed colour parameter values similar to those found in non-mining tributary samples



513 (e.g. v' at Table 3, or a^* shown at Figure 11). This overlap of value ranges could explain in particular
514 the inability of the 'colour' model to provide satisfactory source discrimination. Nevertheless, results
515 obtained with colour parameter analyses coupled to visual observations highlighted the occurrence
516 of two groups of mining tributary samples (i.e. 'Upstream' and 'Downstream'). The coloration
517 differences (i.e. orange/ 'Upstream' and 'red/Downstream') observed between these two groups
518 could be due to the the fact that on the one hand, the reddish colour does not provide a highly
519 conservative signature as it may be altered by the oxydo-reduction of iron minerals during the
520 periods of submersion of sediments under water. On the other hand, the presence of different types
521 of nickel ores could explain these coloration differences. Indeed, nickel ore formation depends partly
522 on the morphological context, for instance on whether nickel ores are located in a basin, on a plateau
523 or a slope. This morphological context influences the weathering level of peridotites (i.e. laterite
524 profile: red laterites at the top >> yellow laterites >> saprolites >> peridotites at the bottom). In the
525 Thio River catchment, nickel ores from the Thio Plateau mine are 'plateau nickel ores' whereas those
526 from the Camps des Sapins mine are 'slope nickel ores' (Mardhel et al., 2018). No information is
527 provided in the literature on the types of nickel ores that were mined in abandoned mining sites. The
528 red coloration of the 'Downstream' mining tributary samples could then be associated with more
529 altered laterite profiles with a thicker layer of red laterites compared to the 'Upstream' mining
530 tributary samples, which could be associated with a laterite profile with a thinner layer of red
531 laterites.

532 1.7.2. 'Geochemistry' model

533 The 'geochemistry' model based on K provided significant discrimination between sources
534 (Table 2), regardless of the types of nickel ores that may be found in the Thio River catchment. K is a
535 lithological tracer discriminating sediments originating from the erosion of the two dominant
536 lithologies (i.e. peridotite massifs vs. volcano-sedimentary formations) in the Thio River catchment.
537 As anthropogenic erosion (i.e. due to mining activities) dominates on the peridotite massifs (Garcin



538 et al., 2017), K therefore provides an optimal discrimination between mining and non-mining
539 tributary contributions.

540 This parameter classified the source samples rather well (i.e. 95.3 % of correct classification,
541 Table 3). Indeed, the 16 mining source samples were all correctly classified (100%) and only one non-
542 mining source sample was not correctly classified (87.5 %); it corresponds to the Watou tributary
543 sample (Figure 11). This sample showed a K content similar to that found in mining tributary samples.
544 The Watou tributary is particular because it drains both volcano-sedimentary formations and
545 peridotite massifs that were not exploited for mining, which justifies that it was considered as a non-
546 mining tributary. The K content measured in this sample could be representative of that found in
547 sediment sources characterized by a mix between the two dominant lithologies. Again, when
548 observing Figure 11, two mining tributary samples (i.e. 'Thio upstream') showed similar K contents to
549 that found in the Watou tributary sample. The 'Thio upstream' tributary also drains both areas
550 associated with volcano-sedimentary formations and exploited peridotite massifs (i.e. mining
551 prospection), which justifies that it was considered as a mining tributary.

552 The analysis of colour parameters coupled with that of geochemical elements indicated that
553 these samples collected on the 'Thio upstream' tributary showed a less red coloration not because
554 they are associated with a different type of ore, as could be the case for the samples collected on
555 Koua tributary draining Camps des Sapins mine (Figure 11), but because they are characterized by a
556 mix of both lithologies. As a result, the 'geochemistry' model showed a certain limitation to classify
557 source samples characterized by a mix of both lithologies. The performance of the 'geochemistry'
558 model described in Table 2 remains, however, excellent. The application of this model on artificial
559 mixture samples provided very satisfactory results (Figure 3-a) with a good correlation between the
560 predicted and the actual source proportions ($r^2= 0.99$). An overestimation of mining tributary
561 contributions is, however, to be taken into account. It was evaluated to a maximum at 15.5 %. This



562 overestimation is greater when the mining contributions estimated by the model tend towards 0 %
563 (maximum: 15.5 %, Figure 3-a).

564 1.7.3. 'Colour + geochemistry' model

565 The 'colour + geochemistry' (i.e. K, Ca, Ti, b*, C*) model provided the best discrimination
566 between sources (Table 3). The inclusion of colour parameters in the 'colour + geochemistry'
567 approach allowed for the discrimination of source samples (i.e. 100 % of correctly classified source
568 samples) that a 'geochemistry' approach alone could not achieve. Results of the tests carried out on
569 the artificial mixture samples also showed an excellent correlation between the predicted and the
570 actual source proportions (i.e. $r^2=0.98$). A slight overestimation of the mining tributary contributions
571 (7 %) was observed with this approach, which remains rather reasonable (Figure 3-b). In this model, K
572 is the lithological tracer which has the higher discriminant powerful (Table 2), which may explain the
573 similarity of results obtained with the 'colour + geochemistry' and the 'geochemistry' models.
574 Indeed, mining tributaries contributed an average of 65 % (SD 27 %) for 'colour + geochemistry'
575 model and 68 % (SD 25 %) for 'geochemistry' model (Table 4). For the 2017 flood event, mining
576 source contributions largely dominated the sediment production with a mean contribution of 83 %
577 (SD 8 %) for the 'geochemistry' model and 88 % (SD 8 %) for the 'colour + geochemistry' model.

578 1.7.4. FDVS-PLSR models

579 The FDVS-PLSR models built from artificial mixture samples showed excellent theoretical
580 predictive performances (e.g. r^2 , RMSEC, RMSEC, Figure 5). However, the application of these models
581 on river sediment samples provided questionable results. Indeed, the artificial mixture samples did
582 not cover entirely the ranges of values found in all sources samples, thus resulting in an
583 overestimation (i.e. superior to 100 %) and an underestimation (i.e. inferior to 0 %) of source
584 composition (Figure 9) in several source samples. Similarly to what was previously observed, three
585 sub-groups of mining tributary samples can be distinguished, one of which (i.e. 'Thio Upstream') is
586 partially merged with the non-mining tributary samples (Figure 9). When modelling the source



587 contributions with the FDVS-PLSR models, a bias was created because the contributions of this
588 mining tributary may be mainly considered as the contributions of non-mining tributaries. As a result,
589 an overestimation of non-mining tributary contributions may be found in the entire Thio River
590 catchment and particularly in the upper part of the study area. Third, the properties measured in the
591 Koua tributary (i.e. draining Camps des Sapins Mine) samples were not comprised in the ranges of
592 values covered by the artificial mixture samples (Figure 9).

593 Given the particular colour signature of this tributary (Figure 11), its contributions are
594 therefore not taken into account at all by the FDVS-PLSR models. Indeed, the sums of the source
595 contributions by FDVS-PLSR models are lower than the expected 100% particularly in the uppermost
596 part of the catchment (Tables 4 and 5), which may indicate that a source is not accounted for.
597 Artificial mixtures were constructed from a homogenized spectral signature of all mining source
598 samples. However, two distinct spectral signatures were observed between the upstream and
599 downstream mining source samples. Homogenizing the spectral signature of the mining samples led
600 to a loss of information in terms of spectral signature, in particular that of the mining samples
601 located upstream. As a result, a 3-source FDVS-PLSR models (i.e. non-mining, upstream and
602 downstream mining sources) would have been more appropriate than 2-source FDVS-PLSR models in
603 this context.

604 **1.8.Spatial and temporal variations of sediment source contributions**

605 Among the four models tested in this study, the 'colour + geochemistry' model is the most
606 appropriate to estimate mining and non-mining tributary contributions in the Thio River catchment.
607 According to the results of this model, mining tributaries provided the main sediment supply to the
608 river system with a mean contribution of 68 % (SD 25 %) for the 2015 flood event and 88 % (SD 8 %)
609 for the 2017 flood event (Tables 4 and 5). The variability of mining tributary contributions between
610 these two flood events with a return period of 10 years ($3500 \text{ m}^3 \text{ s}^{-1}$) could be explained in particular
611 by the variability of rainfall distribution (Sellier et al., 2019). Indeed, during the 2015 flood event, the



612 Kouaré River sub-catchment received twice the rainfall than observed in the rest of the Thio River
613 catchment, which may explain a higher contribution of non-mining tributaries for this event than for
614 the 2017 flood event where rainfall was more intense on the eastern part of the catchment in the
615 vicinity of the mines currently in operation (Thio Plateau, Camps des Sapins).

616 Although the FDVS-PLSR models were unable to properly estimate the source contributions,
617 they provided qualitative indications about the proportion of sediment contribution between
618 'Upstream' and 'Downstream' mining tributaries at the level of the estuary. Indeed, only
619 'downstream' mining tributaries were finally identified by the FDVS-PLSR models as mining sources.
620 Mining contributions gradually increased in downstream direction. The predicted proportion sums of
621 river sediment samples also tend to reach the expected 100%, which could result in a better
622 predictability of the models. As a result, these models indicated that sediment contribution from
623 downstream reaches dominated that of upstream reaches at the level of the estuary for both events.

624 Moreover, the analysis of colour parameters coupled to that of geochemical elements
625 highlighted the occurrence of three sub-groups of mining tributary samples, (1) 'Downstream'
626 samples characterized by high a^* values and low K contents, (2) 'Koua tributary' samples located in
627 the upstream characterized by low a^* values and low K contents and (3) 'Thio upstream' samples
628 corresponding to a mix of both dominant lithologies (i.e. peridotite massifs and volcano-sedimentary
629 formations) characterized by low a^* values and higher K contents (i.e. 4 times higher than for the
630 two previous sub-groups) (Figure 11). Owing to the low K contents found in Thio River sediment
631 samples collected in the uppermost part (i.e. $\sim 2200 \text{ mg kg}^{-1}$ in 2015 and $\sim 2600 \text{ mg kg}^{-1}$ in 2017),
632 which were similar to those measured in samples of sub-group (2, $\sim 2400 \text{ mg kg}^{-1}$), it would appear
633 that the Koua tributary draining Camps des Sapins mine dominated the sediment supply in the
634 upstream for both events.



635 Conclusions

636 The current study showed that the contributions of mining sources dominated the sediment
637 inputs with mean contributions of 68 % (SD 25 %) for the 2015 flood event and 88 % (SD 8 %) for the
638 2017 flood event (results of ‘colour + geochemistry’ model). Although the spatial variability of rainfall
639 may impact local sediment source contributions, a trend in terms of sediment source contributions is
640 observed along the Thio River for both flood events. In the uppermost part of the catchment, mining
641 source contributions dominated (99% in 2015, 100% in 2017) with a dominant contribution from the
642 Koua tributary draining the Camps des Sapins mine. The first non-mining tributary encountered in
643 downstream direction (i.e. the Kouergoa tributary) contributed little to sediment supply; it is rather
644 the next non-mining tributaries (i.e. the Kouaré tributary) which provided most of the sediment
645 inputs (83 % in 2015, 26 % in 2017). Nevertheless, these contributions were compensated in
646 downstream direction by those from mining sources generated by tributaries draining Thio Plateau
647 mine. Finally, at the estuary, mining sources dominated (58-70% in 2015, 83-85 % in 2017). These
648 results therefore suggest that catchment management should focus on mining tributaries draining
649 active mining sites (i.e. Camps des Sapins and the Thio Plateau).

650 One of the objectives of this study was to evaluate the performance of sediment tracing
651 methods based on spectroscopy measurements (i.e. colour parameters and FDVS). The results
652 showed that these individual fingerprinting approaches did not provide sufficient discrimination
653 between sources to be used for the modelling of sediment source contributions. Nevertheless, the
654 inclusion of colour properties in addition to geochemical parameters turned out to be the optimal
655 combination of tracers providing the highest discrimination between sediment sources. This ‘colour +
656 geochemistry’ model is, however largely based on the discriminatory power provided by K, which
657 means that the ‘geochemistry’ approach is also relevant to quantify sediment sources. Both
658 approaches have, moreover, been experimentally validated. As a result, the use of these approaches
659 could be extended to other mining catchments of New Caledonia but also to other similar nickel



660 mining catchments (i.e. Ni oxidized ores based on peridotite massifs) around the world (e.g.
661 Australia, Brazil, Dominican Republic, Cuba).

662 **Data availability**

663 The database has been registered on the PANGAEA website and is currently undergoing the editorial
664 process: <https://issues.pangaea.de/browse/PDI-25229>.

665 Author contribution

666 Oldrich Navratil, Michel Allenbach and Olivier Evrard designed research. Virginie Sellier, Oldrich
667 Navratil, Olivier Evrard and Irène Lefèvre carried out fieldwork sampling. Virginie Sellier conducted the
668 analyses. All co-authors contributed to data analysis and interpretation. John Patrick Laceby
669 contributed to modelling. All co-authors contributed to the writing and approved the final version of
670 the manuscript.

671 Competing interests

672 The authors declare that they have no conflict of interest.

673 **Acknowledgements**

674 This work was funded by the National Technical Research Center (CNRT) “Nickel and Its
675 Environment”, Noumea, New Caledonia » (n°10PS2013-CNRT.UNC/IMMILA). The PhD project of
676 Virginie Sellier is also financed by the French Atomic Energy Commission (CEA, Commissariat à
677 l’Energie Atomique et aux Energies Alternatives). The authors are grateful to Jean-Guy M’Boueri,
678 Pierre Chanel, Jean-Jean, Lorenza M’Boueri, Nicole Mathys for their invaluable support to identify
679 and have access to the field sampling sites.

680



681 References

- 682 Abel, A., Michael, A., Zartl, A., and Werner, F.: Impact of erosion-transported overburden dump
683 materials on water quality in Lake Cospuden evolved from a former open cast lignite mine south of
684 Leipzig, Germany, *Environmental Geology*, 39, 683-688, 2000.
- 685 Baudrimont, M., Dominique, Y., Feurtet-Mazel, A., Gonzalez, P., Gourvès, P.-Y., Gunkel-Grillon, P.,
686 Laporte-Magoni, C., Lefrançois, E., Letourneur, Y., Marquié, J., Maury-Brachet, R., Monna, F.,
687 Pasquet, C., Rivière, E., and Roth, E.: - Rapport scientifique final. Programme « Dispersion des métaux
688 de la mine au lagon. ». CNRT « Nickel & son environnement ». 192 pages, 2019.
- 689 Bird, E. C. F., Dubois, J. P., and Iltis, J. A.: The impacts of opencast mining on the rivers and coasts of
690 New Caledonia. Tokyo, Japan, United Nations University, 1984.
- 691 Blake, W. H., Wallbrink, P. J., Wilkinson, S. N., Humphreys, G. S., Doerr, S. H., Shakesby, R. A., and
692 Tomkins, K. M.: Deriving hillslope sediment budgets in wildfire-affected forests using fallout
693 radionuclide tracers, *Geomorphology*, 104, 105-116, 10.1016/j.geomorph.2008.08.004, 2009.
- 694 Bradley, S., and Lewin, J.: Transport of heavy metals on suspended sediments under high flow
695 conditions in a mineralised region of Wales, *Environmental Pollution Series B, Chemical and Physical*,
696 4, 257-267, 1982.
- 697 Brosinsky, A., Foerster, S., Segl, K., and Kaufmann, H.: Spectral fingerprinting: sediment source
698 discrimination and contribution modelling of artificial mixtures based on VNIR-SWIR spectral
699 properties, *Journal of soils and sediments*, 14, 1949-1964, 2014.
- 700 Collins, A., Walling, D., and Leeks, G.: Use of the geochemical record preserved in floodplain deposits
701 to reconstruct recent changes in river basin sediment sources, *Geomorphology*, 19, 151-167, 1997.
- 702 Collins, A. L., Walling, D. E., and Leeks, G. J. L.: Composite fingerprinting of the spatial source of fluvial
703 suspended sediment : a case study of the Exe and Severn river basins, United Kingdom,
704 *Géomorphologie*, 2, 41-53, 10.3406/morfo.1996.877, 1996.
- 705 Danloux, J., and Laganier, R.: Classification et quantification des phénomènes d'érosion, de transport
706 et de sédimentation sur les bassins touchés par l'exploitation minière en Nouvelle Calédonie, 1991.
- 707 Daszykowski, M., Walczak, B., and Massart, D.: Representative subset selection, *Analytica chimica*
708 *acta*, 468, 91-103, 2002.
- 709 Debret, M., Sebag, D., Desmet, M., Balsam, W., Copard, Y., Mourier, B., Susperrigui, A.-S., Arnaud, F.,
710 Bentaleb, I., and Chapron, E.: Spectrocolorimetric interpretation of sedimentary dynamics: the new
711 "Q7/4 diagram", *Earth-Science Reviews*, 109, 1-19, 2011.
- 712 Dumas, P., Printemps, J., Mangeas, M., and Luneau, G.: Developing erosion models for integrated
713 coastal zone management: A case study of The New Caledonia west coast, *Marine Pollution Bulletin*,
714 61, 519-529, 2010.
- 715 Evrard, O., Lacey, J. P., Huon, S., Lefèvre, I., Sengtaheuanghoung, O., and Ribolzi, O.: Combining
716 multiple fallout radionuclides (^{137}Cs , ^7Be , $^{210}\text{Pbxs}$) to investigate temporal sediment source
717 dynamics in tropical, ephemeral riverine systems, *J Soils Sediments*, 16, 1130-1144, 10.1007/s11368-
718 015-1316-y, 2015.
- 719 Evrard, O., Durand, R., Foucher, A., Tiecher, T., Sellier, V., Onda, Y., Lefèvre, I., Cerdan, O., and
720 Lacey, J. P.: Using spectrocolourimetry to trace sediment source dynamics in coastal catchments
721 draining the main Fukushima radioactive pollution plume (2011–2017), *Journal of Soils and*
722 *Sediments*, 1-12, 2019.
- 723 Evrard, O., Chaboche, P.-A., Ramon, R., Foucher, A., and Lacey, J. P.: A global review of sediment
724 source fingerprinting research incorporating fallout radiocesium (^{137}Cs), *Geomorphology*, 107103,
725 2020.
- 726 Garcin, M.: Exploitation des granulats en lit vif des cours d'eau de la Grande-Terre, Nouvelle-
727 Calédonie. BRGM/RP-58531-FR. 114 p., 90 fig., 3 tabl., Bureau des Recherches Géologiques et
728 Minières 2010.



- 729 Garcin, M., Gastaldi, Y., and Lesimple, S.: Quantification et évolution temporelle des apports miniers
730 dans les rivières calédoniennes. BRGM/RP-66840-FR, 44 p., 23 fig., 5, Bureau des Recherches
731 Géologiques et Minières
- 732 2017.
- 733 Hedouin, L., Pringault, O., Metian, M., Bustamante, P., and Warnau, M.: Nickel bioaccumulation in
734 bivalves from the New Caledonia lagoon: Seawater and food exposure, *Chemosphere*, 66, 1449-1457,
735 2007.
- 736 Highley, D., Chapman, G. R., and Bonel, K.: The economic importance of minerals to the UK, British
737 Geological Survey, 2004.
- 738 Iltis, J.: La mine, élément de la controverse écologique dans le Pacifique Sud, *L'Espace géographique*,
739 193-205, 1992.
- 740 Juillot, F.: – Rapport scientifique final. Programme « Dynamique des métaux de la mine au lagon ».
741 CNRT « Nickel & son environnement ». 202 pages., 2019.
- 742 Klages, M., and Hsieh, Y.: Suspended Solids Carried by the Gallatin River of Southwestern Montana:
743 II. Using Mineralogy for Inferring Sources 1, *Journal of Environmental Quality*, 4, 68-73, 1975.
- 744 Laceby, J. P., and Olley, J.: An examination of geochemical modelling approaches to tracing sediment
745 sources incorporating distribution mixing and elemental correlations, *Hydrol. Process.*, 29, 1669-
746 1685, 10.1002/hyp.10287, 2015.
- 747 Laceby, J. P., Evrard, O., Smith, H. G., Blake, W. H., Olley, J. M., Minella, J. P. G., and Owens, P. N.: The
748 challenges and opportunities of addressing particle size effects in sediment source fingerprinting: A
749 review, *Earth-Sci. Rev.*, 169, 85-103, 10.1016/j.earscirev.2017.04.009, 2017.
- 750 Legout, C., Poulenard, J., Nemery, J., Navratil, O., Grangeon, T., Evrard, O., and Esteves, M.:
751 Quantifying suspended sediment sources during runoff events in headwater catchments using
752 spectrophotometry, *J Soils Sediments*, 13, 1478-1492, 10.1007/s11368-013-0728-9, 2013.
- 753 Mardhel, V., Iseppi, M., Regninger, P. A., and Sevin, B.: Connaissance de l'ophiolite, géophysique
754 aéroportée et étude de la structure. Rapport scientifique final. Programme «OPHIOSTRUCT». CNRT
755 «Nickel & son environnement», 2018.
- 756 Martínez-Carreras, N., Udelhoven, T., Krein, A., Gallart, F., Iffly, J. F., Ziebel, J., Hoffmann, L., Pfister,
757 L., and Walling, D. E.: The use of sediment colour measured by diffuse reflectance spectrometry to
758 determine sediment sources: application to the Atert River catchment (Luxembourg), *J Hydrol*, 382,
759 49-63, 2010.
- 760 Pascal, N.: Ecosystèmes coralliens de Nouvelle-Calédonie. Valeur économique des services
761 écosystémiques. Partie I: Valeur financière. IFRECOR., 2010.
- 762 Poulenard, J., Perrette, Y., Fanget, B., Quetin, P., Trevisan, D., and Dorioz, J.-M.: Infrared
763 spectroscopy tracing of sediment sources in a small rural watershed (French Alps), *Science of the*
764 *Total Environment*, 407, 2808-2819, 2009.
- 765 Poulenard, J., Legout, C., Nemery, J., Bramorski, J., Navratil, O., Douchin, A., Fanget, B., Perrette, Y.,
766 Evrard, O., and Esteves, M.: Tracing sediment sources during floods using Diffuse Reflectance
767 Infrared Fourier Transform Spectrometry (DRIFTS): A case study in a highly erosive mountainous
768 catchment (Southern French Alps), *Journal of Hydrology*, 414, 452-462, 2012.
- 769 Prior, T., Daly, J., Mason, L., and Giurco, D.: Resourcing the future: Using foresight in resource
770 governance, *Geoforum*, 44, 316-328, 2013.
- 771 Rossel, R. V., Walvoort, D., McBratney, A., Janik, L. J., and Skjemstad, J.: Visible, near infrared, mid
772 infrared or combined diffuse reflectance spectroscopy for simultaneous assessment of various soil
773 properties, *Geoderma*, 131, 59-75, 2006.
- 774 Sellier, V., Navratil, O., Laceby, J. P., Allenbach, M., Lefèvre, I., and Evrard, O.: Investigating the use of
775 fallout and geogenic radionuclides as potential tracing properties to quantify the sources of
776 suspended sediment in a mining catchment in New Caledonia, South Pacific, *Journal of Soils and*
777 *Sediments*, 1-17, 2019.



778 Shellberg, J., Brooks, A., and Spencer, J.: Land-use change from indigenous management to cattle
779 grazing initiates the gulying of alluvial soils in northern Australia, 19th World Congress of Soil
780 Science: Soil Solutions for a Changing World, 2010, 1-6,
781 Sherriff, S. C., Franks, S. W., Rowan, J. S., Fenton, O., and Ó'hUallacháin, D.: Uncertainty-based
782 assessment of tracer selection, tracer non-conservativeness and multiple solutions in sediment
783 fingerprinting using synthetic and field data, *J Soils Sediments*, 15, 2101-2116, 10.1007/s11368-015-
784 1123-5, 2015.
785 Smith, H. G., Sheridan, G. J., Lane, P. N. J., Noske, P. J., and Heijnis, H.: Changes to sediment sources
786 following wildfire in a forested upland catchment, southeastern Australia, *Hydrol. Process.*, 25, 2878-
787 2889, 10.1002/hyp.8050, 2011.
788 Surell, A.: Étude sur les torrents des Hautes-Alpes, Carilian-Goeury, 1841.
789 Tiecher, T., Caner, L., Minella, J. P., and dos Santos, D. R.: Combining visible-based-color parameters
790 and geochemical tracers to improve sediment source discrimination and apportionment, *Sci Total*
791 *Environ*, 527-528, 135-149, 10.1016/j.scitotenv.2015.04.103, 2015.
792 Uber, M., Legout, C., Nord, G., Crouzet, C., Demory, F., and Poulénard, J.: Comparing alternative
793 tracing measurements and mixing models to fingerprint suspended sediment sources in a mesoscale
794 Mediterranean catchment, *Journal of Soils and Sediments*, 1-19, 2019.
795 Vaithyanathan, P., Ramanathan, A., and Subramanian, V.: Transport and distribution of heavy metals
796 in Cauvery River, *Water, Air, and Soil Pollution*, 71, 13-28, 1993.
797 Walden, J., Slattery, M. C., and Burt, T. P.: Use of mineral magnetic measurements to fingerprint
798 suspended sediment sources: approaches and techniques for data analysis, *Journal of Hydrology*,
799 202, 353-372, 1997.
800 Wallbrink, P., Murray, A., Olley, J., and Olive, L.: Determining sources and transit times of suspended
801 sediment in the Murrumbidgee River, New South Wales, Australia, using fallout ¹³⁷Cs and ²¹⁰Pb,
802 *Water Resour Res*, 34, 879-887, 1998.
803 Wallbrink, P. J.: Quantifying the erosion processes and land-uses which dominate fine sediment
804 supply to Moreton Bay, Southeast Queensland, Australia, *Journal of environmental radioactivity*, 76,
805 67-80, 2004.
806 Walling, D., Peart, M., Oldfield, F., and Thompson, R.: Suspended sediment sources identified by
807 magnetic measurements, *Nature*, 281, 110, 1979.
808 Yellishetty, M., Mudd, G. M., and Shukla, R.: Prediction of soil erosion from waste dumps of opencast
809 mines and evaluation of their impacts on the environment, *International Journal of Mining,*
810 *Reclamation and Environment*, 27, 88-102, 2013.

811